References

[1]Drummond, J. P., and Hussaini, M. Y., "A Detailed Numerical Model of a Supersonic Reacting Mixing Layer," AIAA Paper 86-1427, June 1986.

[2]Riggins, D. W., and McClinton, C. R., "A Computational Investigation of Flow Losses in a Supersonic Combustor," AIAA Paper 90-2093, July 1990.

[3]Eklund, D. R., Northam, G. B., and Hartfield, R. J., "A Detailed Investigation of Staged Normal Injection into a Mach 2 Flow," 27th JANNAF Combustion Meeting, F. E. Warren Air Force Base, Cheyenne, WY, Nov. 1990.

[4]Eklund, D. R., Northam, G. B., and Fletcher, D. G., "A Validation Study of the SPARK Navier-Stokes Code for Nonreacting Scramjet Combustor Flowfields," AIAA Paper 90-2360, July 1990.

[5]Drummond, G. B., "A Two-Dimensional Numerical Simulation of a Supersonic, Chemically Reacting Mixing Layer," NASA TM 4055, Dec. 1988.

[6]Hitch, B. D., and Senser, D. W., "Reduced H_2-O_2 Mechanisms for Use in Reacting Flow Simulation," AIAA Paper 88-0732, Jan. 1988.

Current Distribution on Isothermal Rod Electrodes in Combustion MHD Generators

Richard P. Heydt*

SRI International, Menlo Park, California 94025

Introduction

ELECTRODE geometry influences MHD generator performance and strongly affects current distribution. This Note summarizes measurements of current distribution made on rod-shaped electrodes in the Stanford M-2 MHD generator. The measurements reported here are several years old, but remain unique for combustion MHD power generation.

In segmented-Faraday generators, with flat, flush-mounted electrodes, current concentrates at the upstream edges of anodes and downstream edges of cathodes, because the axial electric field created by segmentation is locally shorted at the electrode surface. Current concentrations enhance electrode surface erosion and play a major role in interelectrode, axial-field breakdown, through direct heating of the electrode-insulator interface and local heating of the plasma at the electrode surface.

These problems may be alleviated if flat electrodes are replaced with transverse rod electrodes, raised slightly off the generator electrode wall. The rod geometry may be especially useful in suppressing insulator-breakdown arcs, as rod electrodes and interelectrode insulators are in contact in only a small region along the generator sidewall. Since there are no insulator-electrode edges perpendicular to the flow direction, rods can also eliminate concentrations, while distributing current over a larger total area.

Rod electrodes have been studied computationally[1] and experimentally[2] in nonequilibrium generators. No experimental measurements of current distribution have been reported for either combustion or nonequilibrium generators.

The purpose of this research was to determine how load current is distributed on a rod electrode in a combustion MHD generator. It is important to distinguish between the effects of geometry and temperature variations along the electrode circumference, particularly when the plasma flowfield is complex, as with an array of rods. The experimental intent was to produce a near-isothermal rod surface, so that the measured current distributions would primarily represent the effect of electrode shape.

Measurement results are presented in this Note along with predictions from a current-distribution model.

Received Jan. 21, 1994; revision received Sept. 12, 1994; accepted for publication Oct. 3, 1994.

*Research Engineer.

Experiment Description

The experiments were run in the M-2 facility at Stanford University. The fuel was ethanol-seeded with potassium hydroxide, and was burned in oxygen, with nitrogen added as diluent.

Figure 1 illustrates the layout and dimensions of the MHD test section. There were 13 electrode pairs, with the bottom electrode of each pair being a rod. For experimental practicality, the rods were artificially large (a realistic rod-diameter-to-channel-height ratio might be 0.01 or 0.02). One of the rod electrodes was divided into eight segments for current-distribution measurement. Each segment had independent surface-temperature control.

The current distributions reported here are applied-field measurements. Voltage was applied across the top, flat electrode and the bottom, segmented-rod electrode in the presence of magnetic field and plasma flow. Each distribution represents an average of two to five measurements. Current density was kept low to maintain diffuse transfer at the electrode surface. Table 1 gives approximate values of experimental parameters.

Current-Distribution Model

A diffuse-transport, current-distribution model was developed to evaluate the experimental results. The model[3] is based on the two-dimensional, steady-state MHD electrical and energy equations, which were solved by finite difference. A crucial issue is that the current flow pattern is highly dependent on the spatial variation of plasma conductivity, and thus

Table 1 Nominal experiment parameters

Magnetic flux density	2.5 T
Plasma flow velocity	250 m/s
Plasma temperature	2650 K
Rod segment surface temperatures	800 K ± 50 K
Applied (Faraday) voltage	100–200 V
Rod surface current density	0.1–0.3 A/cm^2

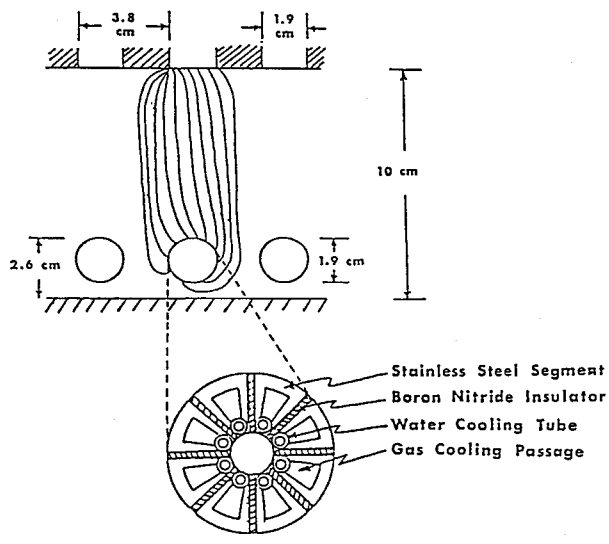

Fig. 1 Side view of the M-2 channel, showing dimensions and a cross section of the segmented rod electrode.

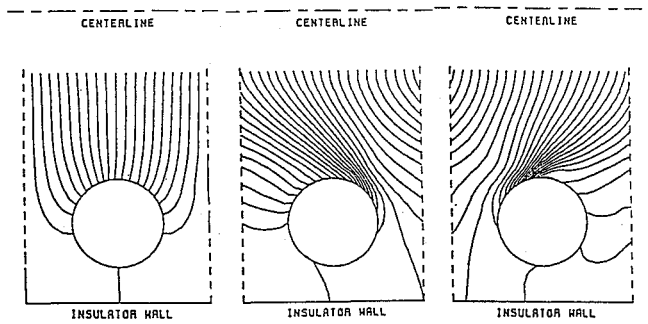

Fig. 2 Predicted current streamlines to a rod electrode without magnetic field (left), cathode polarity with magnetic field (center), and anode polarity with magnetic field (right). Plasma flow is left-to-right and magnetic-field direction is out of the page. Hall parameter is 1.2.

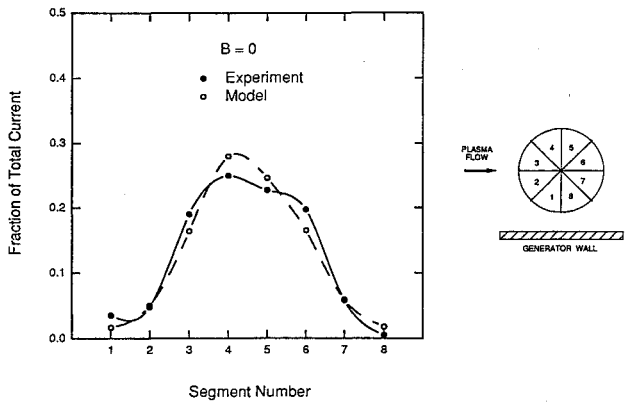

Fig. 3 Measured and predicted current distributions on isothermal rod electrode, for $B = 0$.

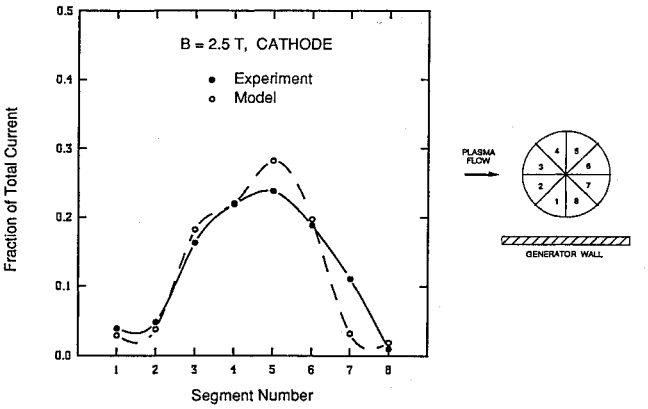

Fig. 4 Measured and predicted current distributions on isothermal rod electrode, for $B = 2.5$ T, cathode polarity.

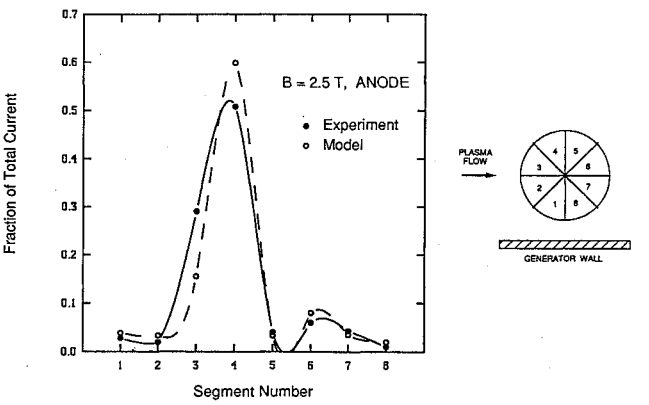

Fig. 5 Measured and predicted current distributions on isothermal rod electrode, for $B = 2.5$ T, anode polarity.

on temperature. The procedure was to solve the energy equation for the temperature field, determine the corresponding plasma-conductivity field, and then solve the electrical equation for the current stream function.

Results

Figure 2 shows predicted current streamlines to the rod electrode for the cases $B = 0$, $B = 2.5$ T with the rod in cathode polarity, and $B = 2.5$ T with the rod in anode polarity.

Figure 3 compares the measured current distribution for $B = 0$, with the electrode in cathode polarity, and the model prediction. The distribution is roughly symmetric on the upstream and downstream sides of the electrode. Although the electrode is isothermal, there is some asymmetry as a result of the stagnation-heating region in the vicinity of segment 4. Approximately 85% of the current enters the top half of the electrode.

When the magnetic field is turned on and the electrode is in cathode polarity (Fig. 4), current shifts to the downstream side. The measured distribution shows a significant increase in current to segment 7. Current that would concentrate at a flat-electrode edge has instead moved to the rod underside. The model prediction in Fig. 4 shows more current remaining on top of the rod. Nevertheless, note the absence of any large concentration; segments 3–6 all carry significant current.

Figure 5 shows the anode-polarity results for $B = 2.5$ T. In contrast to the cathode case, more than 80% of the total current is carried by the upstream segments 3 and 4. The experimentally measured shift is again somewhat greater than the model predicts. However, the basic character of the experimental and model distributions is the same. The fact that the model predicts the concentration in segments 3 and 4 suggests that it is caused by a Hall-effect shift of current into the stagnation-heating region of the rod. It occurs even when the rod surface is isothermal and current transport is diffuse.

The basic profile shapes of the experimental data in Figs. 3–5 were repeatable, and changed only when the surface was forced to be nonisothermal.

Not shown here is the measured $B = 0$ current distribution with the electrode in anode polarity. This distribution was constricted, much more like the $B = 2.5$ T anode distribution (with most of the current in segments 3 and 4) than the $B = 0$ cathode distribution. The apparent constriction instability could have been induced by the cold electrode surface.

Conclusions

Experimental results show that current distribution on rod electrodes in a combustion MHD generator depends strongly on electrode polarity. In the presence of a magnetic field, current on an isothermal rod cathode was distributed more uniformly and over a larger area than on a flat electrode of the same width. However, an isothermal rod anode showed a large current concentration in the vicinity of the stagnation region. A current-distribution model shows that the anode concentration arises because the magnetic field forces current into the stagnation region on the upstream side of the rod. Replacing flat electrodes with rods on the anode wall of a generator is thus unlikely to improve current distribution. Rod-type electrodes may still be advantageous in preventing insulator-initiated, Hall-field breakdown.

References

[1]Houben, J. W. M. A., Blom, J. H., and Rietjens, L. H. Th., "The Effects of Electrode Configuration on the Performance of a Faraday Type MHD Generator," 12th Symposium on the Engineer-

ing Aspects of MHD, Argonne, IL, 1972.
[2]Blom, J. H., Veefkind, A., and Reitjens, L. H. Th., "High Power Density Experiments in the Eindhoven Shocktunnel MHD Generator," 6th International Conf. on MHD Electrical Power Generation, Washington, DC, 1975.
[3]Heydt, R. P., "The Effect of Rod Electrodes on the Performance of Combustion MHD Generators," Ph.D. Dissertation, Dept. of Mechanical Engineering, Stanford Univ., Stanford, CA, Oct. 1985.

Combustion Performance of Bipropellant Liquid Rocket Engine Combustors with Fuel-Impingement Cooling

Tsung Leo Jiang* and Wei-Tang Chiang†
National Cheng Kung University, Tainan, Taiwan 70101, Republic of China
and
Shyh-Dihng Jang‡
Lungtan, Taiwan 32526, Republic of China

Introduction

A NUMBER of computational fluid dynamics (CFD) approach-based comprehensive analytical tools have been recently proposed in providing detailed combustion analyses and in aiding in the thruster design of the modern advanced liquid rocket engine. For instance, Liang et al.[1] successfully analyzed a cryogenic LOX/H_2 rocket engine combustor with a liquid-gas injection. Jiang and Chiu,[2] however, proposed a computational bipropellant spray combustion model, in which both fuel and oxidizer droplet flows were solved, and when certain droplet combustion criteria were satisfied, fuel or oxidizer droplet burning was assumed. Their numerical predictions[2] revealed that finer-droplet sprays do not necessarily lead to a higher combustion efficiency as traditionally speculated. The bipropellant spray combustion model was also applied in analyzing an orbital maneuvering vehicle's (OMV) thrust chamber.[3] This chamber was equipped with a centrally installed pintle-type ring-shaped injector. For such a small in-space propulsive engine combustor, the propellant conversion efficiency was predicted to be relatively low due to poor bipropellant mixing resulting from part of the fuel being injected toward the chamber wall for impingement cooling.

Due to the complexity associated with modeling the expansion nozzle, numerical analyses of liquid bipropellant rocket engine combustors have unanimously been confined within the combustor itself, thereby allowing the effects of the nozzle to be neglected with the chamber pressure being specified as a prior given condition at a point on the injector face. However, the combustion performance of a bipropellant liquid rocket engine thruster can be evaluated only when the chamber pressure is predicted rather than prespecified. Therefore, the flow analysis has to be conducted from the injector face down to at least the propulsive nozzle throat. In the present study, the flow analysis for the axisymmetric thrust chamber of an OMV[3] installed with a pintle-type ring-shaped injector and a conical convergent nozzle is conducted. Liquid monomethyl hydrazine (MMH) and nitrogen tetroxide (NTO) storable bipropellants serve as the fuel and oxidizer sources, respectively, with MMH being assumed injected through the injector toward the chamber wall for impingement cooling. An optimum injected fuel and oxidizer droplet-size combination is suggested based upon the results obtained from a systematic sensitivity study examining the effects of both injected fuel and oxidizer droplet sizes on chamber-wall temperature distributions and the chamber pressure.

Received May 29, 1993; revision received July 14, 1994; accepted for publication Oct. 6, 1994.
*Associate Professor, Institute of Aeronautics and Astronautics.
†Research Assistant, Institute of Aeronautics and Astronautics.
‡Senior Scientist, P.O. Box 90008-15-12. Member AIAA.

Formulation

The present mathematical framework consists of an Eulerian/Eulerian approach[2,3] for gas and liquid-droplet flows. The full axisymmetric compressible Navier-Stokes equations as well as the compressible k-ε two-equation turbulence model are solved for the gas flow. The liquid-droplet flow equations for each droplet-size group consist of the droplet number-density, momentum, and energy equations. For fuel and oxidizer, the inlet droplet number density is assumed to linearly decrease and increase, respectively, as one goes from the outer to the inner rim of the pintle-type ring-shaped injector. With such an injection pattern, fuel impingement cooling at the chamber wall is viable. The choking condition is assumed at the nozzle throat. For such an irregularly shaped combustor, a computer code[4] was specially developed based on body-fitted nonorthogonal grids and employed in analyzing the present compressible turbulent reacting flow. The computational geometric configuration and grid system consisting of 48 × 21 nonuniform staggered grids are depicted in Fig. 1. Convergence is assured by requiring the maximum mass residual of the continuity equation down to prescribed small values and the relative difference of the variables between two iterations smaller than 10^{-4}. More than 3000 iterations are required for a converged calculation.

Results and Discussion

In the present analysis, a fuel-rich injection ratio of 1.64 is presumed, since part of the fuel is assumed to be injected toward the chamber wall for impingement cooling. The ratio of nozzle inlet to throat area is 6.637, and the total mass flow rate is 0.2133 kg/s. The variation in chamber pressure predicted for various injected fuel and oxidizer volume-mean droplet diameters (D_{30}) is depicted in Fig. 2. Chamber pressure is defined as the mean pressure at the injector face. Injected droplet size combinations of 20, 40, 60, 80, and 100 μm and 40, 60, 80, and 100 μm are investigated for $(D_{30})_{ox}$ and $(D_{30})_{fu}$, respectively. For each $(D_{30})_{ox}$ series [different $(D_{30})_{fu}$ values for a constant $(D_{30})_{ox}$ value], best performance in terms of maximum chamber pressure results for the following various $(D_{30})_{fu}$: $40 > 60 > 80 > 100$ μm, except for the 100-μm $(D_{30})_{ox}$ series, where a $(D_{30})_{fu}$ of 80 μm yields the maximum chamber pressure. It is interesting to note that for each $(D_{30})_{fu}$, increasing $(D_{30})_{ox}$ results in a marked increase in chamber pressure to a maximum value at a $(D_{30})_{ox}$ of 80 μm, after which, chamber pressure drops off slowly. This result indicates that for the present thrust chamber and injection pattern, there exists an optimum $(D_{30})_{ox}$ value that achieves the best combustion performance. Excessively small $(D_{30})_{ox}$, however, generally lead to low combustion performance.

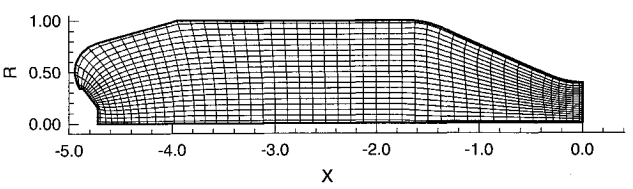

Fig. 1 Computational geometric configuration and grid system of the combustor.